Journal of Materials Synthesis and Processing, Vol. 1, No. 2, 1993

A Model for the Isothermal Isobaric Chemical Vapor Infiltration (CVI) in a Straight Cylindrical Pore. Application to the CVI of SiC

R. Fédou,[1] F. Langlais,[1,2] and R. Naslain[1]

A previously described modeling of the chemical vapor infiltration (CVI) process in a straight cylindrical pore is applied to the deposition of SiC-based ceramics from CH_3SiCl_3–H_2 in the case of a first-order kinetic law with respect to CH_3SiCl_3. The model gives concentrations and deposit thickness profiles along the pore at any stage of the densification and, particularly, at the end of the process when the pore becomes sealed. The infiltration homogeneity is predicted to be improved by decreasing the aspect ratio of the pore and the CVI temperature and, under conditions of Fick diffusion, by decreasing the total pressure and the pore diameter. The model is validated by the good fit between the deposit thickness profiles along the pore calculated after adjustment of the kinetic data and experimental profiles drawn for a 34-μm straight pore.

KEY WORDS: Chemical vapor infiltration; straight cylindrical pore; SiC; numerical model.

1. INTRODUCTION

Silicon carbide (SiC) is more and more often prepared as thin films by chemical vapor deposition (CVD), for its interesting physical and chemical properties. Besides its electronic applications [1], SiC is used as a matrix in fiber-reinforced ceramic–ceramic composites owing to its high thermal, mechanical, and chemical characteristics for applications at high temperatures in oxidizing atmospheres [2]. The chemical vapor infiltration (CVI) technique, which derives directly from CVD, is well adapted to the processing of such ceramic matrix composites: it consists mainly of the densification of a porous fiber preform with a ceramic matrix deposited in situ from a gaseous precursor [3].

If specific cases are excepted [4–13], most SiC depositions involve the Si–C–H–Cl chemical system [2, 14–26]. An organometallic compound, e.g., CH_3SiCl_3 (MTS), is often used as precursor, partly for its ability to be decomposed at moderate temperatures (which usually favors the CVI process) and partly for economic reasons [27, 28].

In order to understand the mechanisms involved in the CVI process and to optimize the homogeneity and rate of the infiltration, a model was built in the case of a single straight cylindrical pore. A detailed description of this model was given in the previous paper, Part 1 [29]. The aim of the present paper, Part 2, is to apply the model to the CVI of SiC in the MTS–H_2 system, to investigate the effect of the experimental parameters on the theoretical deposit thickness and concentration profiles, on the basis of simplified hypotheses concerning the heterogeneous chemical process. Then an experimental procedure in a hot wall reactor is proposed to validate the model and hypotheses on the chemistry are discussed in order to fit the calculated profiles with the experimental data.

2. DATA RELATED TO THE CH_3SiCl_3–H_2 SYSTEM

2.1. The Gaseous Phase

The MTS molecule is known to be rapidly decomposed in the homogeneous phase, particularly in a hot

[1] Laboratoire des Composites Thermostructuraux, UMR 47 CNRS-SEP-UB1, Domaine Universitaire, 3 Allée La Boétie, 33600 Pessac, France.

[2] To whom correspondence should be addressed.

1064-7562/93/0300-0061$07.00/0

wall reactor [30]. But data are not available on either the kinetics of the homogeneous reactions or the actual composition of the gaseous phase close to the deposition surface. So MTS is supposed to react itself heterogeneously according to

$$CH_3SiCl_{3(g)} \xrightarrow{H_2} SiC_{(s)} + 3HCl_{(g)} \qquad (1)$$

This SiC deposition reaction gives rise to a large amount of HCl. As a consequence, the chemical system considered in the present application of the CVI model includes the three gaseous species MTS, H_2, and HCl.

2.1.1. *Diffusion Coefficients*

The Knudsen diffusion coefficient of species i is calculated using Eq. (16) of Part 1 [29], which can be written as

$$D_{i,K} = d_{i,K}\, \Phi\, T^{1/2} \qquad (2)$$

where $d_{i,K}$ is a reduced Knudsen diffusion coefficient which depends only on the molar mass of species i (Table I).

The Fick diffusion coefficients are calculated on the basis of Eq. (15) and Appendix 1 in Part 1 [29]. For binary mixtures including MTS molecules, it is necessary to use Gilliland's expression Eq. (A4) in Ref. [29] rather than that of Hirschfelder Eq. (A1) in Ref. [29] because data such as the collision diameter σ and reduced Lennard–Jones energy ϵ/k are not available for MTS. The data needed to perform the calculations of Fick diffusion coefficients are listed in Tables II and III: σ, ϵ/k, and molar volume v for each species. The molar volume of CH_3SiCl_3 is considered as the sum of the volumes of each atom [31].

Table I. Values of Molar Masses M_i and Reduced Knudsen Diffusion Coefficients $d_{i,K}$

	Species i		
	CH_3SiCl_3	H_2	HCl
M_i(kg · mol^{-1})	0.149	2×10^{-3}	3.65×10^{-2}
$d_{i,K}$(m · s^{-1} · K$^{-1/2}$)	3.97	34.30	8.03

Table II. Values of σ_i and ϵ_i/k Chosen for the Calculation of Ω_D (from Ref. 31)

	Species i	
	H_2	HCl
σ_i(nm)	0.2827	0.3339
ϵ_i/k (K)	59.7	344.7

Table III. Values of Molar Volume Used in the Gilliland Formula (From Ref. 32)

Species i	v_i or Σv_i (cm^3 · mol^{-1})
H_2	14.3
CH_3SiCl_3	122.7
HCl	25.3

2.1.2. *Heterogeneous Kinetics*

The reaction corresponding to Eq. (1) was found by a few authors to exhibit first-order kinetics with respect to MTS under specific conditions [23, 27, 28, 33]. Nevertheless, several results are not in good accordance with such an order and the surface mechanisms involved in this system are not clarified [34–36]. In the present study, a simplified kinetics is used, which assumes a direct reaction of MTS on the solid surface and first order with respect to this species. The kinetic law taken from Schoch *et al.* [37] is the following:

$$\vartheta = k_0 \exp\left(-\frac{E_a}{\mathbf{R}T}\right) C_{MTS} \qquad (3)$$

where $k_0 = 3.89 \times 10^9$ m · s^{-1}, $E_a = 296$ kJ · mol^{-1}, **R** is the ideal gas constant (8.314 J · mol^{-1} K^{-1}), and C_{MTS} is the MTS concentration in the gaseous phase near the reaction surface (in mol · m^{-3}).

2.2. The Deposited Solid

The gaseous mixture MTS–H_2 can yield a codeposition of SiC with free carbon or free silicon under specific conditions. Nevertheless, it is possible to find a large range of experimental conditions which lead to stoichiometric SiC deposit. In the present study, the deposited solid is assumed to be pure SiC without microporosity.

The molar volume V_s of SiC (which is supposed not to depend on the deposition conditions), calculated according to Eq. (21) of Part 1 [29] with a density of 3.2, is equal to 1.25×10^{-5} m^3 mol^{-1}.

2.3. The Boundary Conditions

At the pore entrances, the gaseous phase composition is assumed to be constant and the HCl concentration to be zero:

$$C_{MTS}(0, t) = C_{MTS,0} \qquad (4)$$

$$C_{H_2}(0, t) = C_{H_2,0} \quad (5)$$

$$C_{HCl}(0, t) = 0 \quad (6)$$

As MTS species are not supposed to react homogeneously, the gaseous phase at the entrances of the pore can be defined partly by the ratio α between H_2 and MTS concentrations at the entrance of the reactor:

$$\frac{C_{H_2,0}}{C_{MTS,0}} = \alpha \quad (7)$$

On the other hand, the entrance total concentration can be written as a function of the temperature T and the total pressure P:

$$C_{H_2,0} + C_{MTS,0} = \frac{P}{RT} \quad (8)$$

By combining (7) and (8), it is possible to calculate each entrance concentration with respect to the experimental parameters:

$$C_{MTS,0} = \frac{1}{1 + \alpha} \frac{P}{RT} \quad (9)$$

$$C_{H_2,0} = \frac{\alpha}{1 + \alpha} \frac{P}{RT} \quad (10)$$

3. CALCULATION RESULTS

The model provides the diameter of the pore and the composition of the gaseous phase for any value of the space–time coordinates (z, t) and any infiltration conditions: T, P, and α values at the pore entrance and geometry of the pore (length L and initial diameter Φ_0). The results of the simulation are presented mainly as deposit thickness profiles $\{[\Phi_0 - \Phi(z, t)]/2$, where $\Phi(z, t)$ is the diameter at the abscissa z and the instant $t\}$ in a half-pore (i.e., for $0 \leq z \leq L/2$, with L the length of the pore) at the end of the densification process, i.e., when the pore entrance becomes closed at $t = t_c$. A few examples of gaseous species concentration profiles and plots of the infiltrated volume fraction of SiC versus time are also given.

3.1. Influence of Temperature

Figure 1 shows the influence of temperature on the calculated profiles, for a total pressure of 20 kPa, an initial pore diameter $\Phi_0 = 100$ μm, an initial aspect ratio (L/Φ_0) of 100, and a value of $\alpha = 10$.

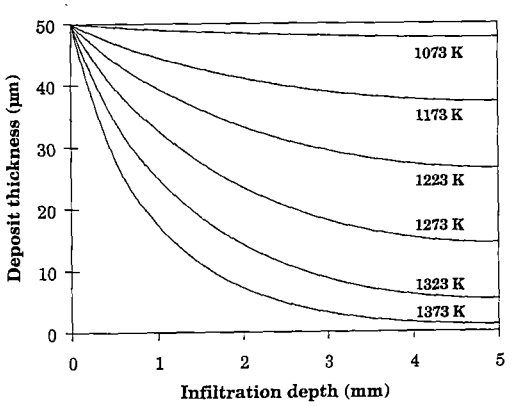

Fig. 1. Influence of temperature on the calculated thickness profiles of a silicon carbide deposit obtained from a MTS–H_2 gas mixture with $P = 20$ kPa, $\Phi_0 = 100$ μm, $L/\Phi_0 = 100$, and $\alpha = 10$.

The infiltration appears to be almost perfectly homogeneous at 1073 K, while at 1373 K only a very thin layer of SiC is deposited at the center of the pore. These results, which depend directly on the high activation energy of the heterogeneous kinetics, are qualitatively similar to those presented in previous works [3, 26, 38].

3.2. Influence of Total Pressure

The influence of total pressure is shown in Figs. 2 and 3 for a temperature of 1223 K, an initial aspect ratio of 100, a gaseous phase composition defined by $\alpha = 10$, and a respective diameter of 100 and 1 μm (which means a respective length of 10 and 0.1 mm). In order to compare the behavior of both types of pores, the reduced infiltration depth $z' = z/L$ is needed [29]. In the

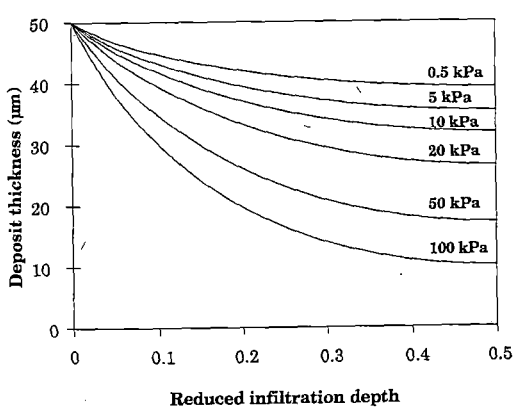

Fig. 2. Influence of total pressure under the Fick diffusion regime on the calculated thickness profiles of a silicon carbide deposit obtained from a MTS–H_2 gas mixture with T = 1223 K, $\Phi_0 = 100$ μm, $L/\Phi_0 = 100$, and $\alpha = 10$.

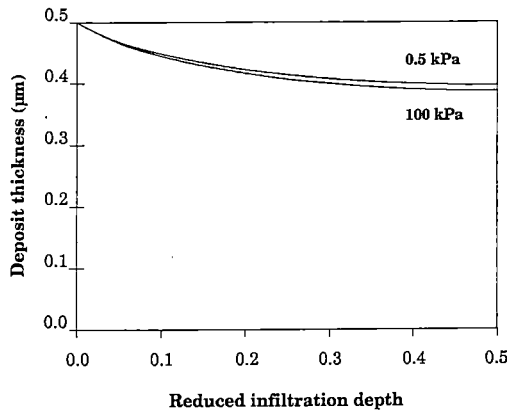

Fig. 3. Influence of total pressure under the Knudsen diffusion regime on the calculated thickness profiles of a silicon carbide deposit obtained from a MTS–H_2 gas mixture with T = 1223 K, Φ_0 = 1 μm, L/Φ_0 = 100, and α = 10.

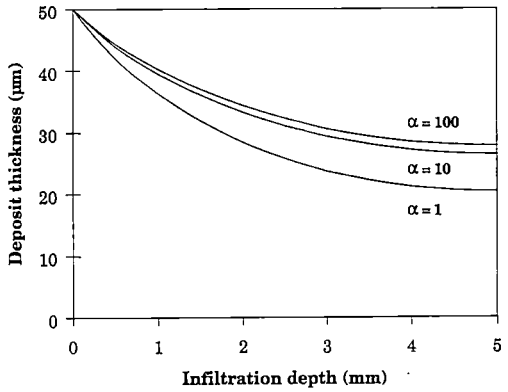

Fig. 4. Influence of external composition of the gas phase (α ratio = $[H_2]/[MTS]$) on the calculated thickness profiles of a silicon carbide deposit obtained from a MTS–H_2 gas mixture with T = 1223 K, P = 20 kPa, Φ_0 = 100 μm, L/Φ_0 = 100, and $1 \leq \alpha \leq 100$.

first case (i.e., for a large pore where the mass transfers occur mainly by Fick diffusion), a decrease in the total pressure from 100 to 10 kPa drastically improves the infiltration homogeneity, but a further decrease from 10 to 0.5 kPa should not be very useful. The latter feature can be explained by assuming that, as the pressure decreases, the Knudsen regime becomes predominant and the effect of pressure on the reaction rate and the diffusion transfer are balanced. This independence of the infiltration profiles from the total pressure in the Knudsen regime is confirmed in the case of small pores, where a pressure decrease from 100 to 0.5 kPa results in a very low profile change. This independence can be explained on the basis of the Thiele modulus, a dimensionless number characterizing the homogeneity of a deposit in a cylindrical pore for a reaction order of one (the infiltration profiles are more homogeneous with a smaller Thiele modulus) [29]:

$$\tau = \sqrt{\frac{k_s L^2}{D\Phi_0}} \qquad (11)$$

where k_s is the kinetic constant of the heterogeneous reaction (in m · s^{-1})

For the Fick diffusion regime, the diffusion coefficient D is proportional to P^{-1} and τ is proportional to $P^{1/2}$. So a decrease in P leads to a decrease in τ, which means an improvement of the infiltration profile.

Under the Knudsen diffusion regime, D and, consequently, τ do not depend on the total pressure, which does not affect the infiltration profiles.

3.3. Influence of the Gas Phase Composition at the Pore Entrance

Deposit thickness profiles are plotted in Fig. 4 for three values of the external composition ratio α, T = 1223 K, P = 20 kPa, Φ_0 = 100 μm and L/Φ_0 = 100 (i.e., under the Fick diffusion regime). The small differences between these profiles can be attributed to the dependence of the MTS Fick diffusion coefficient on the composition of the gas phase. This coefficient is a combination of the MTS–H_2 and MTS–HCl binary mixture coefficients, with the molar fractions of H_2 and HCl, according to Eq. (15) in Ref. 29. When MTS species are highly diluted in hydrogen, i.e., for a high α ratio ($10 \leq \alpha \leq 100$), D_{MTS} is very close to D_{MTS,H_2} and the calculated profile in the pore is hardly influenced by the external composition of the gas phase. For a more concentrated gaseous mixture ($1 \leq \alpha \leq 10$), the HCl molar fraction within the pore is relatively high and $D_{MTS,HCl}$, which is lower than D_{MTS,H_2}, must be taken into account. As α decreases from 10 to 1, an increase in the HCl concentration results in a decrease in D_{MTS} and a degradation of the infiltration profile.

Generally speaking, the low dependence of the deposit thickness profiles on the gas phase composition originates in the first order of the deposition reaction rate. The case of more complex kinetic laws will be studied in Part 3 [39].

3.4. Influence of the Pore Geometry

The influence of the geometry of the pore is presented in Figs. 5 to 7. It can be analyzed on the basis

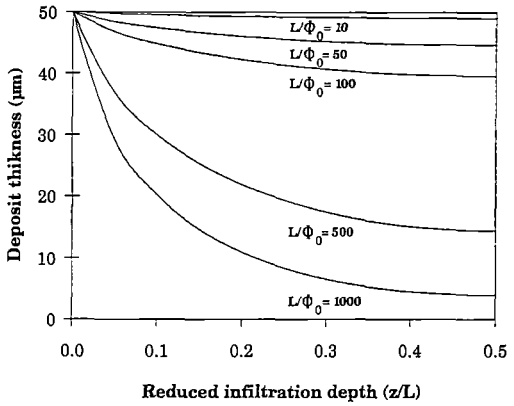

Fig. 5. Influence of the aspect ratio on the calculated thickness profiles of a silicon carbide deposit obtained from a MTS–H_2 gas mixture with T = 1223 K, P = 0.1 kPa, Φ_0 = 100 μm, and α = 10.

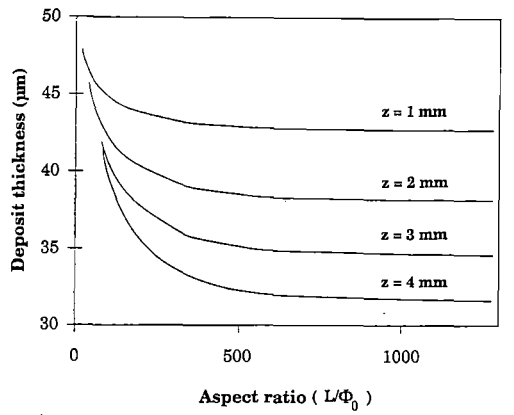

Fig. 6. Influence of the aspect ratio on the deposit thickness at $t = t_c$ and at a given infiltration depth z (with $1 < z < 4$ mm) in a cylindrical pore for silicon carbide infiltration with T = 1223 K, P = 0.1 kPa, Φ_0 = 100 μm, and α = 10.

of the Thiele modulus reexpressed as follows:

$$\tau = \frac{L}{\Phi_0}\,\Phi_0^{1/2}\sqrt{\frac{k_s}{D}} \qquad (12)$$

with two geometrical parameters, the aspect ratio L/Φ_0 and the pore diameter Φ_0.

Figure 5 shows the influence of the aspect ratio L/Φ_0 on the calculated thickness profiles for T = 1223 K, P = 0.1 kPa, α = 10, and Φ_0 = 100 μm. As the aspect ratio increases from 10 to 1000, i.e., the pore length varies from 1 to 100 mm, the infiltration profiles (drawn with the reduced infiltration depth as the abscissa) are less and less homogeneous, particularly for high values of the aspect ratio.

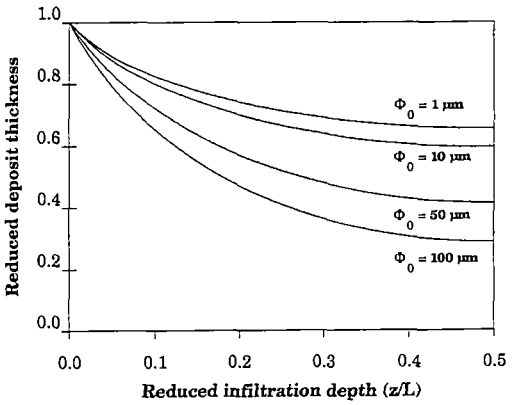

Fig. 7. Influence of the diameter on the calculated thickness profiles of a silicon carbide deposit obtained from a MTS–H_2 gas mixture with T = 1273 K, P = 20 kPa, L/Φ_0 = 100, and α = 10.

Figure 6 shows the variations of the deposit thickness at a given infiltration depth and at the end of the densification (i.e., for $t = t_c$), as a function of the aspect ratio, under the same conditions as those for Fig. 5. For high values of the aspect ratio, the chosen infiltration depths (1 to 4 mm) are close to the entrance of the pore. The deposit thickness decreases rapidly when L/Φ_0 rises to 500, but beyond this value the variations are rather flat, i.e., the phenomena occurring near the pore entrance are not significantly influenced by the length of the pore. The first part of these plots can be explained as follows: an increase in the aspect ratio provides a larger area available for the heterogeneous reaction, which leads to a more important consumption of MTS species per unit time, i.e., a higher MTS molar diffusional flux at the pore entrance and, consequently, an increase in the MTS concentration and deposit thickness gradients.

The influence of the pore diameter Φ_0 (with a constant aspect ratio) on the infiltration profiles is shown in Fig. 7, plotting the reduced deposit thickness $[\Phi_0 - \Phi(z, t_c)]/\Phi_0$ versus the reduced infiltration depth, under the following conditions: T = 1223 K, P = 20 kPa, α = 10, and L/Φ_0 = 100. A decrease in the pore diameter improves the homogeneity of the infiltration profile, which is in accordance with a decrease in the Thiele modulus [Eq. (12)], but the improvement is not so important for small pores ($1 \leq \Phi_0 \leq 10$). In the latter case, as the pore diameter decreases, the mass transfers occur more and more by Knudsen diffusion, the diffusion coefficient D becomes proportional to the diameter Φ_0, and the Thiele modulus and the infiltration profile become independent of the diameter (for a constant aspect ratio).

3.5. Concentration and Deposit Thickness Profiles During Densification

As the model permits calculation of the deposit thickness and the gas phase concentrations at any stage of the infiltration process, it is interesting to simulate how densification occurs as a function of time. The conditions chosen are the following: $T = 1223$ K, $P = 100$ kPa, $\Phi_0 = 100$ μm, $L/\Phi_0 = 100$, and $\alpha = 10$.

Figure 8 shows the various profiles for four values of infiltration time (including the last, $t = t_c$). The thickness gradient is steeper and steeper close to the pore entrance as the densification process is going on (Fig. 8a). On the other hand, the gaseous species concentration profiles (Fig. 8b) exhibit a simultaneous decrease in MTS concentration and increase in HCl concentration from the entrance to the center of the pore. The concentration gradients are increased during infiltration, particularly at the end of the process (i.e., between $t = 0.75t_c$ and $t = t_c$). Moreover, it is noteworthy that the gas phase near the center of the pore is rather poor in MTS, while the HCl concentration is almost as high as that of MTS at the entrance of the pore. These results are directly related to the rather poor thickness profiles shown in Fig. 8a.

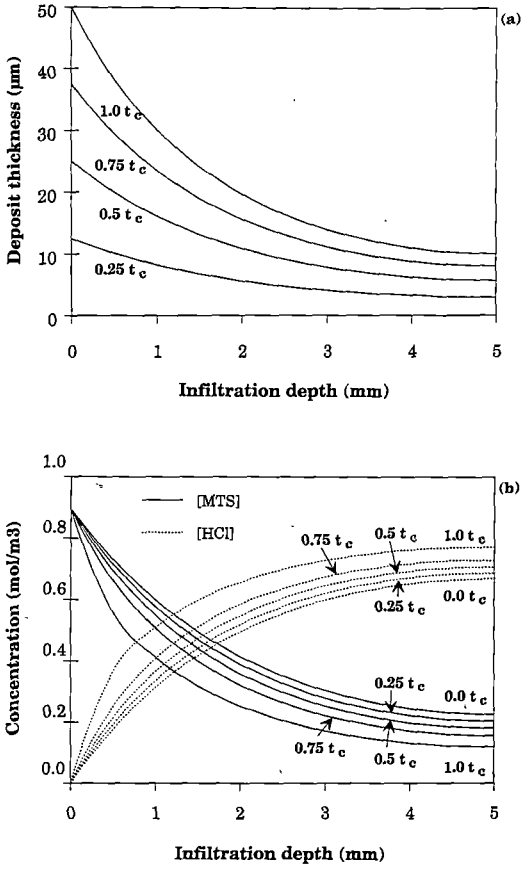

Fig. 8. Calculations of (a) deposit thickness profile and (b) concentrations of the gaseous species profiles for a silicon carbide deposit obtained from a MTS–H_2 gas mixture and for various infiltration times between $t = 0$ and $t = t_c$ with $T = 1223$ K, $P = 100$ kPa, $\Phi_0 = 100$ μm, $L/\Phi_0 = 100$, and $\alpha = 10$.

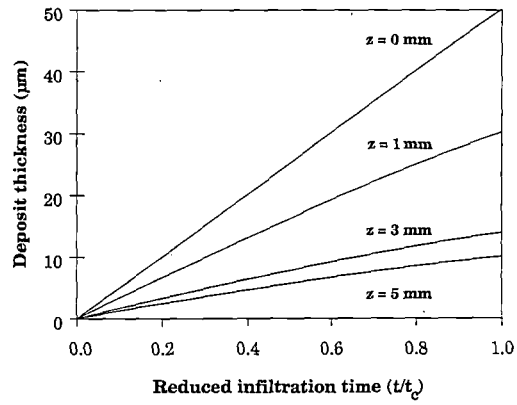

Fig. 9. Variations of the deposit thickness with the reduced time at various infiltration depths for a silicon carbide deposit obtained from a MTS–H_2 gas mixture with $T = 1223$ K, $P = 100$ kPa, $\Phi_0 = 100$ μm, $L/\Phi_0 = 100$, and $\alpha = 10$.

The deposit thickness can also be plotted versus reduced time as shown in Fig. 9 for various infiltration depths from the entrance ($z = 0$) to the center ($z = 5$ mm) of the pore. As densification proceeds, the local deposition rate decreases within the pore, particularly at the center, while it is constant at the entrance.

Another way to simulate the pore densification is to plot versus reduced time the volume fraction of infiltrated silicon carbide, as defined by

$$\eta(t) = \frac{2}{L}\int_0^{L/2} \frac{\Phi_0^2 - \Phi^2(z, t)}{\Phi_0^2}\, dz \qquad (13)$$

Such infiltration curves are shown in Fig. 10 for various values of the aspect ratio in the range 10–1000 and an initial diameter of 100 μm. As the aspect ratio increases, particularly from 100 to 1000, the SiC volume fraction obtained when the pore is closed is markedly decreased, which is consistent with the degradation of the corresponding thickness profiles. Nevertheless, this type of description of the infiltration process hides the actual shape of the profile, because many $\Phi(z)$ functions can yield the same volume fraction of infiltrated SiC.

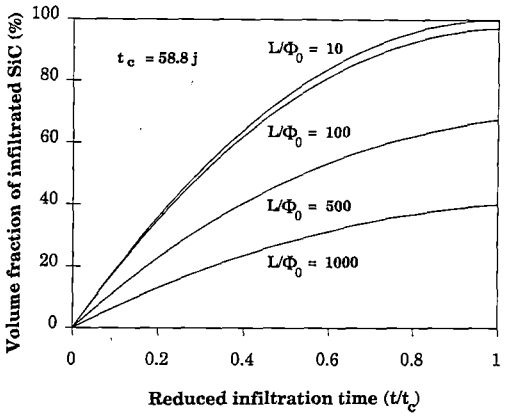

Fig. 10. Variations of the volume fraction of infiltrated SiC with the reduced time for $T = 1223$ K, $P = 0.1$ kPa, $\Phi_0 = 100$ μm, $\alpha = 10$, and various values of the aspect ratio.

4. EXPERIMENTAL STUDY

Until now, few papers have reported experimental thickness profiles for ceramics obtained by CVI. This is probably due to problems occurring in (i) the preparation of model pores with a well-controlled geometry and which conveniently represent the pores of the actual fibrous preforms of the ceramic matrix composites (low diameter, < 100 μm, and high aspect ratio, > 100) and (ii) the accurate measurement of deposit thicknesses of about 1 μm. The only articles published in this field give qualitative profiles (obtained by electron probe for microanalysis) for the infiltration of TiC [38] or zirconia [40, 41] in ceramic fibrous preforms or quantitative thickness profiles of SiC or TiC in a capillary about 1 mm in diameter with a low aspect ratio (< 100) [33, 42, 43].

4.1. Preparation of the Model Pores

The preparation route used to obtain straight cylindrical pores started with cylindrical SiC-based CVD filaments (SCS-2 filaments from TEXTRON, Lowell, MA), which consist of (i) a carbon core (32 μm in diameter), (ii) a pyrocarbon coating (about 1 μm in thickness), and (iii) a 53-μm SiC deposit. Pieces of these filaments (about 1 cm in length) were subjected to controlled oxidation at 800°C in air for about 10 h, which resulted, by consumption of the carbon core and pyrocarbon film, in a microscopic tube with an inner diameter of 34 μm. These samples, briefly characterized by optical and scanning electronic microscopy (SEM), were found to be very regular, with a smooth inner surface (Fig. 11). Several of these unitary pores were bound together with a high-temperature cement and the resulting assembly was hung up in a CVD/CVI reactor, with the direction of the pores axis perpendicular to the gas flow (Fig. 12).

4.2. CVI Experiments

The infiltration experiments were carried out in a hot wall CVD/CVI apparatus heated by r.f. induction (Fig. 13). The deposition chamber is a vertical cylindrical tube favorable to a laminar flow, with a large hot isothermal zone, coupled to a sensitive microbalance. It is equipped with accurate controlling systems for the monitoring of temperature, total pressure, and various flow rates. MTS (which is liquid under standard conditions) is transported by bubbling the carrier gas H_2 in a bubbler vessel at a constant temperature. Good control of the MTS gas flow requires some additional devices, which are described elsewhere [34].

4.3. Experimental Results—Discussion

The CVI experiments were performed during a sufficiently long time to close the pore entrances. The thickness profiles were determined by SEM observations on fracture sections operated at various levels in the model micropores (Fig. 14). The experimental parameters studied are the temperature ($1073 \leq T \leq 1373$ K), the total pressure ($2 \leq P \leq 20$ kPa), and the aspect ratio ($90 \leq L/\Phi_0 \leq 300$).

4.3.1. Influence of the Aspect Ratio

The influence of the aspect ratio was experimentally studied under two CVI conditions. The first investigation was performed for $T = 1073$ K, $P = 3$ kPa, $\alpha = 3$, and two values of pore length ($L = 10$ and 5 mm, corresponding to respective aspect ratios of 300 and 150). In spite of relatively favorable conditions, the SiC thickness profiles are not very homogeneous, as shown in Fig. 15. The volume fractions of infiltrated SiC are, respectively, 63 and 81%. The second investigation, for $T = 1223$ K, $P = 10$ kPa, $\alpha = 5$, and three values of pore length ($L = 10$, 5, and 3 mm, i.e., $L/\Phi_0 = 300$, 150, and 90), gives similar results with still less homogeneous profiles (Fig. 16). In both sets of experiments, an increase in the aspect ratio leads to a degradation of the infiltration profile, which is qualitatively in agreement with the results of the model (Fig. 5).

Nevertheless, according to the kinetic law defined

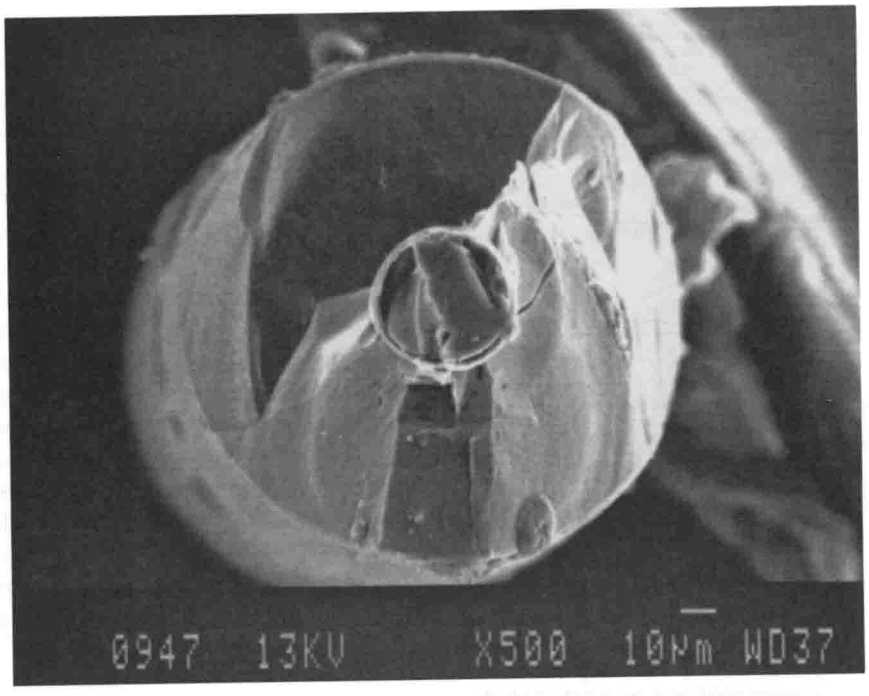

(a)

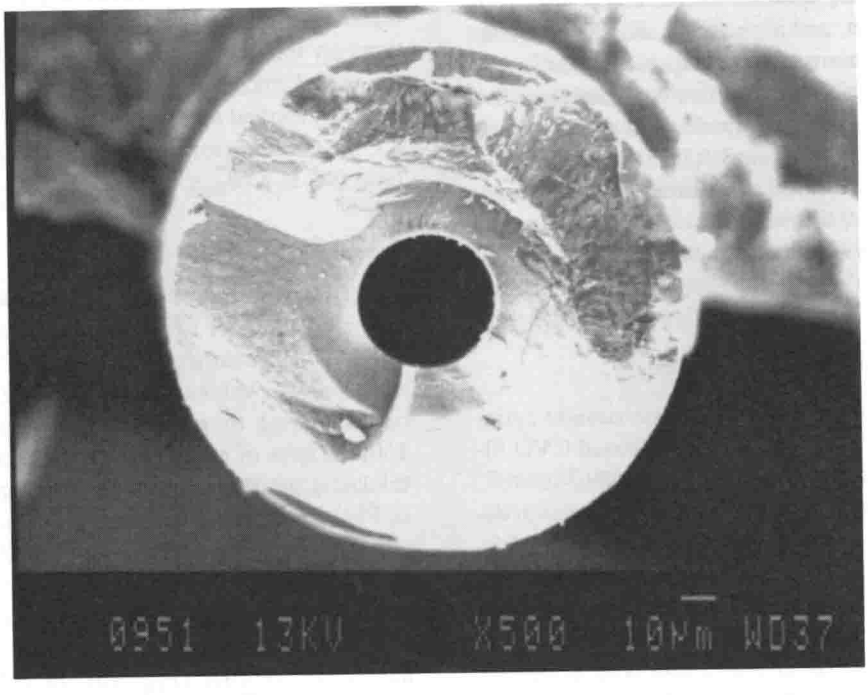

(b)

Fig. 11. SEM micrographs of fracture surfaces of SiC-based CVD filaments: (a) as received; (b) after oxidation treatment.

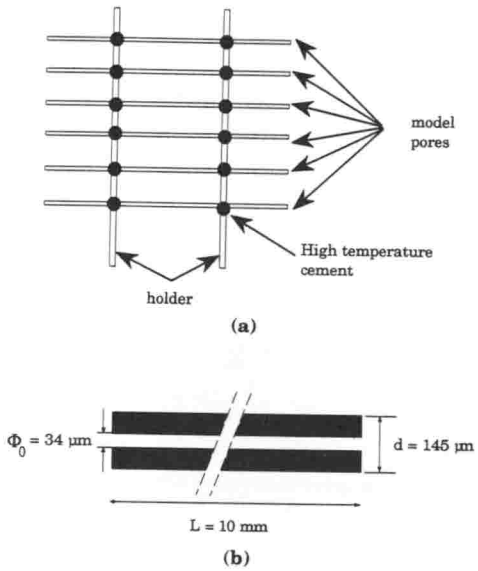

Fig. 12. Model samples for experimental determination of silicon carbide thickness profiles along a model cylindrical pore: (a) model pore assembly; (b) pore geometry.

in Section 2.1.2 [Eq. (3)] for the deposition of SiC, the theoretical profiles calculated from the present model are much more optimistic than the experimental profiles, with a volume fraction of infiltrated SiC higher than 99%. As mentioned previously, the assumption stated in Section 2.1 about the chemical system (i.e., the heterogeneous reaction of MTS) is not valid and one (or even several) intermediate unknown species X, homogeneously produced, must be considered as the actual source of SiC deposit at the entrance of the pore. The concentration of species X is probably much lower than the initial concentration of MTS because the decomposition of MTS yields, besides X, several other species which do not react heterogeneously. So the rate of the deposition reaction can be expressed at the pore entrance:

$$\vartheta = k_{s1}(T)\,C_{MTS,0} = k_{s2}(T)\,C_{X,0} \tag{14}$$

where $C_{MTS,0}$ is the MTS concentration at the pore entrance according to the hypotheses in Section 2.1 [i.e. defined by Eq. (9)], $C_{X,0}$ is the actual X concentration at the pore entrance, $k_{s1}(T)$ is the kinetic constant of Eq. (3), and $k_{s2}(T)$ is a new kinetic constant more convenient for representing the deposition chemical process.

The kinetic constant $k_{s2}(T)$ can be expressed as a function of $k_{s1}(T)$:

$$k_{s2} = \frac{C_{MTS,0}}{C_{X,0}}\,k_{s1} \tag{15}$$

with $C_{MTS,0} > C_{X,0}$.

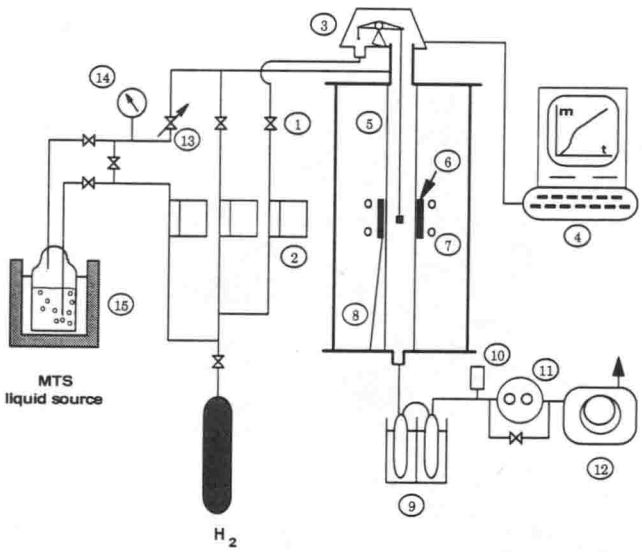

Fig. 13. Schematics of the apparatus used for CVD/CVI of SiC-based ceramics. Notation: 1, shut-off valve; 2, mass flowmeter; 3, microbalance; 4, microcomputer; 5, silica tubular reactor; 6, susceptor; 7, r.f. coil; 8, thermocouple; 9, liquid nitrogen trap; 10, pressure sensor; 11, pressure controller; 12, vacuum pump; 13, adjusting valve; 14, manometer ($P°$); 15, thermostated bath ($P°_{MTS}$).

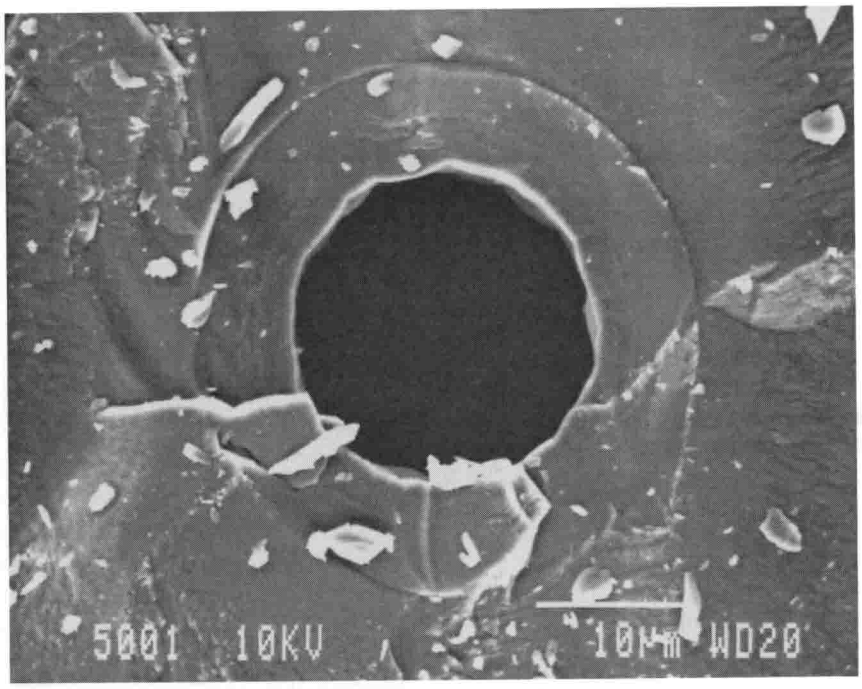

(a)

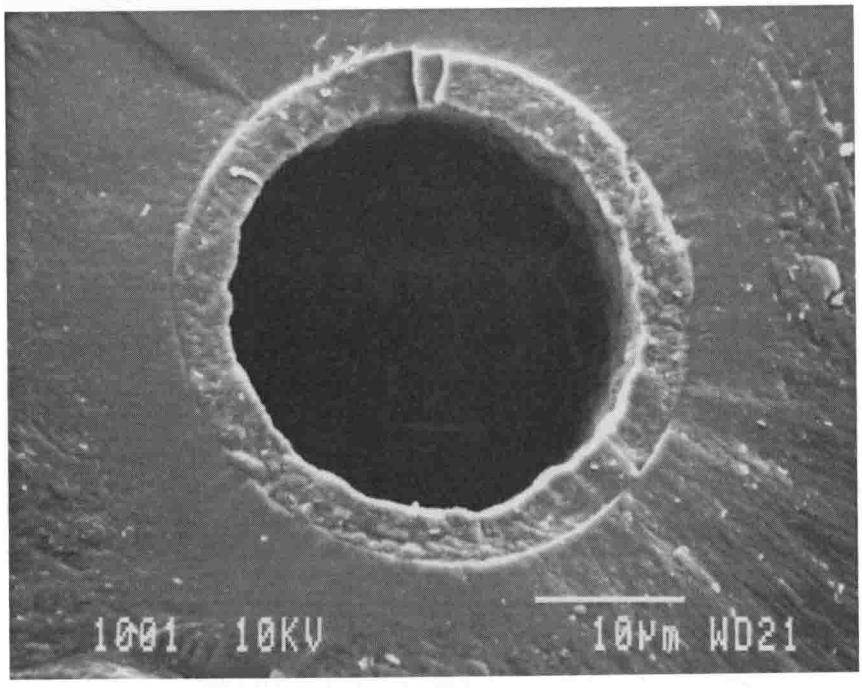

(b)

Fig. 14. SEM micrographs of fracture sections operated at various levels on model pores infiltrated by SiC (a) at 1.5 mm and (b) at 5 mm from the pore entrance.

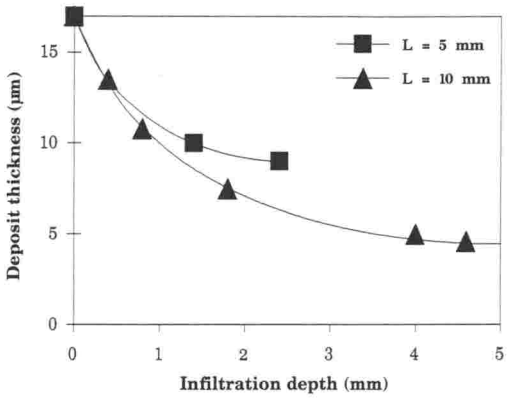

Fig. 15. Calculated (solid lines) and experimental (symbols) thickness profiles along a cylindrical pore for silicon carbide infiltrations with T = 1073 K, P = 3 kPa, Φ_0 = 34 μm, L = 10 and 5 mm, and α = 3.

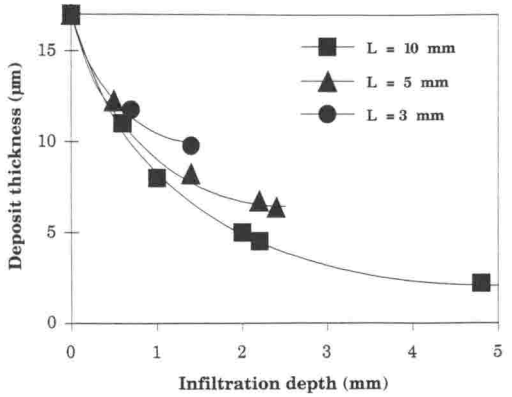

Fig. 16. Calculated (solid lines) and experimental (symbols) thickness profiles along a cylindrical pore for silicon carbide infiltrations with T = 1223 K, P = 10 kPa, Φ_0 = 34 μm, L = 10, 5, and 3 mm, and α = 5.

The value of this ratio has been determined in order to fit one experimental profile from the first investigation (Fig. 15). The chosen value of 30 seems very suitable since for both aspect ratios it leads to calculated profiles very close to the experimental profiles. In addition, the same procedure, permitted very good fitting of the three experimental infiltration profiles from the second investigation (Fig. 16). These results show that the present model can accurately predict the influence of the aspect ratio on the deposit profiles, when a convenient kinetic law for the heterogeneous reaction is available.

4.3.2. *Influence of Total Pressure*

Figure 17 shows three thickness profiles measured after infiltrations at T = 1223 K, α = 5, and L = 10 mm, for three values of total pressure, P = 2, 10, and 20 kPa. Such conditions are favorable to mass transfers occurring within the pore by Fick diffusion. Under this type of mass transfer regime, the model predicts, with the kinetic law defined in Section 2.1.2, an improvement of the infiltration homogeneity when P is decreased. Nevertheless, these experimental profiles are observed to be almost independent of P, which is not in accordance with the previsions of the model (Fig. 2).

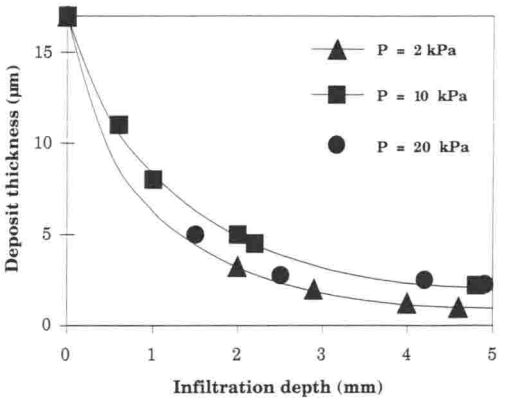

Fig. 17. Calculated (solid lines) and experimental (symbols) thickness profiles along a cylindrical pore for silicon carbide infiltrations with T = 1223 K, P = 2, 10, and 20 kPa, Φ_0 = 34 μm, L = 10 mm, and α = 5.

This behavior could be explained on the basis of a Thiele modulus which does not depend on the total pressure. This condition would be achieved if the kinetic law were a first-order law with respect to the intermediate X with a kinetic constant proportional to P^{-1}. A kinetic law taking into account the inhibitor effect of HCl species can be expressed by the following general expression:

$$\vartheta = \frac{k_1 C_X}{1 + k_2 C_{HCl}} \tag{16}$$

This inhibitor effect of HCl was observed previously by Bessmann *et al.* [44]. On the other hand, Prébendé reported a clear decrease in SiC deposition rate under similar experimental conditions for a total pressure increasing from 3 to 15 kPa (Fig. 18) [34].

HCl is a product of the homogeneous decomposition of MTS, occurring outside the pore, e.g., according to the equation [34]

$$CH_3SiCl_3 + H_2 \longrightarrow CH_4 + SiCl_2 + HCl \tag{17}$$

So the HCl concentration at the pore entrance is close to the MTS concentration ($C_{MTS,0}$) defined by Eq. (9).

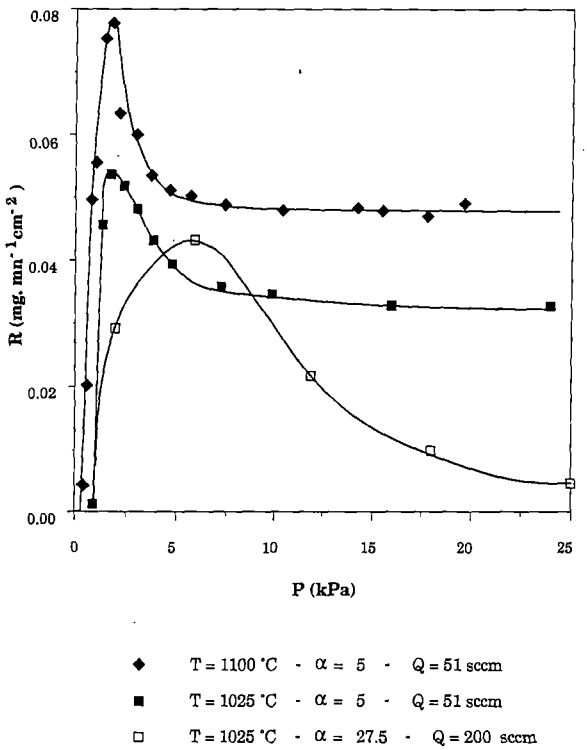

Fig. 18. Variations of the growth rate of silicon carbide deposit from a MTS–H_2 gas mixture [34].

HCl is also a product of the heterogeneous deposition reaction in the pore. As suggested by Fig. 8b, the increase in the HCl concentration from the entrance ($C_{HCl,0}$) to the center of the pore is usually lower than the concentration of the source species at the pore entrance. Equation (15) shows that the condition $k_{s2} \gg k_{s1}$, required to get a good fitting between theoretical and experimental profiles, results in $C_{X,0} \ll C_{MTS,0}$. Consequently, the concentration of HCl is almost constant within the pore and Eq. (16) can be rewritten as

$$\vartheta(z, t) = \frac{k_1 C_X(z, t)}{k_2 C_{HCl,0}} \tag{18}$$

$C_{HCl,0}$ being proportional to the initial concentration of MTS; i.e., for a constant α ratio, proportional to the total pressure, the kinetic law (18) can be reduced to a first-order law with respect to intermediate species X with a kinetic constant proportional to P^{-1}:

$$\vartheta(z, t) = \frac{k_3}{P} C_X(z, t) \tag{19}$$

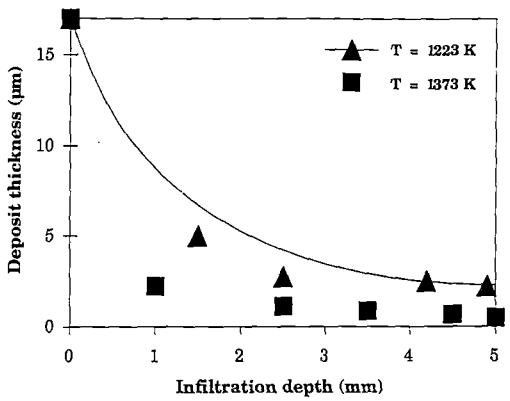

Fig. 19. Calculated (solid lines) and experimental (symbols) thickness profiles along a cylindrical pore for silicon carbide infiltrations with $T = 1223$ and 1373 K, $P = 20$ kPa, $\Phi_0 = 34$ μm, $L = 10$ mm, and $\alpha = 5$.

With such a kinetic law for SiC deposition reaction, the independence of the infiltration profiles on the total pressure for the previously mentioned CVI conditions could be predicted by the model.

4.3.3. Influence of Temperature

The experimental data shown in Fig. 19 for infiltrations performed at $P = 20$ kPa, $\alpha = 5$, and $L = 10$ mm, and for $T = 1223$ and 1373 K, are in qualitative agreement with the profiles calculated by the model with the kinetic law defined in Section 2.1.2 (Fig. 1). A temperature increase results in a degradation of the infiltration profile.

However, a steep thickness gradient is observed close to the pore entrance, over about 1 mm, and thereafter the profile is rather flat. These features, observed mainly at the highest temperature, are not accurately predicted by the model but can be explained on the basis of the inhibitor effect of HCl according to the kinetic law corresponding to Eq. (16). So the increase in HCl concentration as a function of the infiltration depth close to the pore entrance must be added to the decrease in the concentration of the intermediate source species X [assumed to be close, at the pore entrance, to the MTS concentration defined by Eq. (9)], both phenomena leading to a decrease in the heterogeneous reaction rate, particularly at high temperatures. As a consequence of this inhibitor effect, the thickness gradient is enhanced near the pore entrance compared to the theoretical profile calculated under the assumption of a first-order kinetic law. Thereafter, the lower values of the heterogenous reaction rate result in rather low variations of the

various gaseous species concentrations along the pore and an almost-flat thickness profile.

5. CONCLUSION

The CVI model for the infiltration of a straight cylindrical pore, described in Part 1 [29], has been applied here to the deposition of SiC-based ceramics from MTS–H_2 mixtures.

On the basis of a simplified kinetic law, first order with respect to MTS, the model brings out the influence of various parameters on the CVI process. The infiltration homogeneity is highly improved by decreasing the pore aspect ratio (with a constant diameter) and the temperature (due to the large activation energy of the kinetic process) and, in the case of the Fick diffusion regime, by decreasing the total pressure and the pore diameter (with a constant aspect ratio). Conversely, the composition of the gaseous phase (i.e., the ratio $\alpha = [H_2]/[MTS]$) and, in the case of the Knudsen diffusion regime, the total pressure and the diameter have a very weak influence on the deposit thickness profiles.

The infiltration experiments carried out in model pores (34 μm in diameter and 10 mm in length) permit validation of the CVI model by predicting the influence of the aspect ratio accurately, when suitable chemical kinetic data are considered. For instance, at relatively low temperatures and in order to take into account that the actual species which reacts heterogeneously is an intermediate species rather than MTS, the kinetic constant must be adjusted to a higher value in accordance with first-order kinetics and a lower concentration of the intermediate. On the other hand, the experiments performed for various temperatures and total pressures show that a kinetic law more complex than a first-order one must be considered, which includes an inhibitor effect of HCl species.

The investigations carried out in the present study emphasize the importance of the kinetic data used in CVI models and, particularly, the need for a good knowledge of the homogeneous and heterogeneous chemical processes and the local kinetic laws, i.e., with respect to the intermediate source species.

ACKNOWLEDGMENTS

This work was supported by the EEC (EURAM Program Contract MAIE/0018/C) and jointly by the French Ministry of Research and Technology (MRT) and the SEP through a grant to R.F.

REFERENCES

1. J. A. Powell and L. G. Matus, in *Proc. First Int. Conf. Amorph. Crystal. Silicon Carbide*, G. L. Harris and C. Y.-W. Yang, eds. (Springer-Verlag, Berlin/Heidelberg, 1989), p. 2.
2. F. Christin, R. Naslain, and C. Bernard, in *Proc. 7th Int. Conf. CVD, Los Angeles, USA (1979)*, T. O. Sedgwick *et al.*, eds. (Electrochem. Soc., Princeton, NJ, 1979), pp. 499–514.
3. R. Naslain, F. Langlais, and R. Fedou, in *Proc. 7th Eur. Conf. CVD, Perpignan, France (1989)*, M. Ducarroir *et al.*, eds. (Colloque de Physique, Les Editions de Physique, Colloque C5, Suppl. No. 5, Vol. 50, 1989), pp. 191–207.
4. P. Rai-Choudhury and N. P. Formigoni, *J. Electrochem. Soc.* **116,** 1440 (1969).
5. J. E. Doherty, *J. Metals* **28,** 6 (1976).
6. R. Rampuch and L. Stobierski, *Ceramung. Int.* **3,** 43 (1977).
7. A. Suzuki *et al.*, *J. Crystal Growth* **70,** 287 (1984).
8. S. Motojima *et al.*, *J. Mater. Sci.* **121,** 1363 (1986).
9. Y. Furumura, M. Doki, F. Mieno, T. Eshita, T. Suzuki, and M. Maeda, in *Proc. 10th Int. Conf. CVD*, G. W. Cullen, ed. (Electrochem. Soc., Pennington, 1987), p. 435.
10. Y. Avignal, M. Schieber, and R. Levin, *J. Crystal Growth* **24/25,** 188 (1974).
11. F. Sibieude and G. Benezech, *J. Mater. Sci.* **23**(7), 1632 (1988).
12. H. Matsunami *et al.*, *Proc. First Int. Conf. Amorph. Crystal. Silicon Carbide, Vol. 3* (1957), No. 4, pp. 443–448.
13. L. S. Hong, Y. Shimogaki, and H. Komiyama, in *Proc. 8th Eur. Conf. CVD, Glasgow (1991)*, M. L. Hitchman and N. J. Archer, eds. (Journal de Physique IV, Les Editions de Physique, Colloque C2, Suppl. Journal de Physique II, 1991), Vol. 1, pp. 87–94.
14. T. D. Gulden, *Am. Ceram. Soc.* **51,** 424 (1968).
15. J. J. Federer, *Thin Solid Films* **40,** 89 (1977).
16. K. Minato and K. Fukuda, *J. Nucl. Mater.* **149,** 233 (1987).
17. F. Kobayaski, K. Ikawa, and K. Iwamoto, *J. Crystal Growth* **28,** 395 (1975).
18. P. Tsui and K. E. Spear, *Mater. Sci. Res.* **17,** 371 (1984).
19. M. G. So and J. S. Chun, *J. Vac. Sci. Technol.* **6,** 5 (1988).
20. B. S. Cartwright and P. Popper, *Sci. Ceram.* **5,** 473 (1970).
21. A. W. C. Van Kemenade and C. F. Stemfoort, *J. Crystal Growth* **12,** 13 (1972).
22. W. F. Knippenberg, G. Verspui, and A. W. C. Van Kemenade, Proc. 3rd Int. Conf. Silicon Carbide (University of South Carolina Press, Columbia, 1974), p. 92.
23. K. Brennfleck, E. Fitzer, G. Schoch, and M. Dietrich, in *Proc. 9th Int. Conf. CVD, Cincinnati, USA (1984)*, McD. Robinson *et al.*, eds. (Electrochem. Soc., Pennington, 1984), p. 649.
24. A. N. Kenigfest *et al.*, *Fiz. Kim. Obrabotki Mater* **18,** 76 (1984).
25. T. Kaneko, T. Onuko, and H. Yumoto, *J. Crystal Growth* **91,** 599 (1988).
26. E. Fitzer and R. Gadow, *Am. Ceram. Soc. Bull.* **65,** 326–335 (1986).
27. J. Schlichting, *Powder Metall. Int.* **12**(3), (1980).
28. J. Schlichting, *Powder Metall. Int.* **12**(4), 196 (1980).
29. R. Fédou, F. Langlais, and R. Naslain, *J. Mater. Synth. Process.* **1,** 43 (1993).
30. J. Yeheskel, S. Agam, and M. S. Darriel, in *Proc. 11th Int. Conf. CVD*, K. E. Spear and G. W. Cullen, eds. (Electrochem. Soc., Pennington, 1990), pp. 699–702.
31. R. A. Svehla, *NASA Tech. Rep. R-132* (Lewis Research Center, Cleveland, Ohio, 1962).

32. E. R. Gilliland, *Ind. Eng. Chem.* **26,** 681 (1934).
33. E. Fitzer and D. Hegen, *Angew. Chem. Int. Ed. Engl.* **18,** 295 (1979).
34. C. Prébendé, Thesis No. 347 (University of Bordeaux I, Bordeaux, 1989).
35. G. S. Fischman and W. T. Petuskey, *J. Am. Ceram. Soc.* **68,** 185 (1985).
36. M. E. Aluko, in *Proc. First Int. Conf. Amorph. Crystal. Silicon Carbide*, G. L. Harris and C. Y.-W. Yang, eds. (Springer-Verlag, Berlin/Heidelberg, 1989), p. 51.
37. G. Schoch, W. Fritz, and E. Fitzer, Tech. Rep. EURAM Contract MAIE/0018/C (1991).
38. J. Y. Rossignol, F. Langlais, and R. Naslain, *Proc. 9th Int. Conf. CVD, Cincinnati, USA (1984)*, J. M. Blocher *et al.*, eds. (Electrochem. Soc., Pennington, 1984), pp. 596–914.
39. R. Fédou, E. Sipp, F. Rebillat, F. Langlais, and R. Waslain, submitted for publication.
40. J. Minet, F. Langlais, and R. Naslain, *Compos. Sci.* **37,** 79 (1990).
41. L. C. J. de Haart *et al.*, *J. Eur. Ceram. Soc.* **8,** 59 (1991).
42. C. H. J. Van Den Brekel *et al.*, in *Proc. 8th Int. Conf. CVD*, J. M. Blocher *et al.*, eds. (Electrochem. Soc., Pennington, 1981), pp. 142–156.
43. M. Sasaki, A. Ohkubo, and T. Hirai, *J. Physique IV, Coll. C2, Suppl. J. Physique II,* **1,** 127 (1991).
44. T. M. Bessmann, B. W. Sheldon, and M. D. Kaster, *J. Am. Ceram. Soc.* (in press).